Title

The circadian dynamics of the hippocampal transcriptome and proteome is altered in experimental temporal lobe epilepsy

Journal

Science Advances, 6(41)

ISSN

2375-2548

Authors

Debski, KJ

Ceglia, N

Ghestem, A

et al.

Publication Date

2020-10-09

DOI

10.1126/sciadv.aat5979

Peer reviewed

NEUROSCIENCE

The circadian dynamics of the hippocampal transcriptome and proteome is altered in experimental temporal lobe epilepsy

K. J. Debski[1,2*†], N. Ceglia[3*], A. Ghestem[4*], A. I. Ivanov[4*], G. E. Brancati[4], S. Bröer[5], A. M. Bot[1], J. A. Müller[6], S. Schoch[6], A. Becker[6], W. Löscher[5], M. Guye[7,8], P. Sassone-Corsi[9], K. Lukasiuk[1], P. Baldi[3], C. Bernard[4‡]

Gene and protein expressions display circadian oscillations, which can be disrupted in diseases in most body organs. Whether these oscillations occur in the healthy hippocampus and whether they are altered in epilepsy are not known. We identified more than 1200 daily oscillating transcripts in the hippocampus of control mice and 1600 in experimental epilepsy, with only one-fourth oscillating in both conditions. Comparison of gene oscillations in control and epilepsy predicted time-dependent alterations in energy metabolism, which were verified experimentally. Although aerobic glycolysis remained constant from morning to afternoon in controls, it increased in epilepsy. In contrast, oxidative phosphorylation increased in control and decreased in epilepsy. Thus, the control hippocampus shows circadian molecular remapping, which is altered in epilepsy. We suggest that the hippocampus operates in a different functioning mode in epilepsy. These alterations need to be considered when studying epilepsy mechanisms, designing drug treatments, and timing their delivery.

INTRODUCTION

Numerous physiological processes and functions are regulated in a circadian manner throughout body organs (*1*). The core mechanism includes the circadian oscillation of large sets of genes and proteins (*1*), which has been extensively characterized in the suprachiasmatic nucleus (SCN). In this brain region, transcriptional and translational feedback loops involving various clock genes/proteins produce daily oscillations of many downstream genes and proteins (*2*, *3*). Although primarily driven by the SCN, the presence of intrinsic oscillating clock genes in many organs results in circadian changes of their molecular landscape, hence of their functions (*1*).

In the mammalian brain, in addition to the SCN, circadian oscillations of genes and proteins are also present in the cerebellum and the brainstem (*4*), raising the possibility of an ubiquitous phenomenon in all brain regions. In keeping with this proposal, the transcriptome, proteome, and phosphorylome of synaptosomes obtained from the whole forebrain display strong dynamical modifications driven by the sleep-wake cycle (*5*, *6*). Whether the molecular architecture of the hippocampus, a brain region involved in many cognitive and memory processes, oscillates in a circadian manner is not known. Since some clock genes are known to exhibit rhythmic expression in the hippocampus (*7*, *8*), we hypothesized that a large set of their target genes and proteins would display circadian rhythmicity. Our first goal was thus to establish which genes and proteins oscillate in the hippocampus in control mice. This knowledge is important to gain because an oscillating molecular landscape may provide a more detailed mechanistic basis for the daily variation in hippocampal physiology, including synaptic responses (*9*), long-term synaptic plasticity (*10*, *11*), place cell firing (*12*), and theta oscillations (*13*).

In pathological conditions, there is a tight relationship between altered circadian molecular oscillations and the phenotypes expressed in various body organs (*1*). Whether and how circadian molecular oscillations are modified in brain disorders are not known. Epilepsy is one of the most common forms of brain disorders. Since the expression and rhythmicity of clock genes are altered in human (*14*) and experimental (*15*) epilepsy, we hypothesized a different molecular oscillating landscape in the hippocampus in experimental temporal lobe epilepsy (TLE), the most common form of adult epilepsy, as compared to control. If this were true, then the circadian molecular landscape of the ventral hippocampus, which is part of the epileptogenic zone in the pilocarpine experimental model of epilepsy (*16*), would be of particular interest. This knowledge is important to gain because it may explain why seizures display a strong circadian rhythmicity (*17*, *18*), shed light on seizure mechanisms, and could be used to improve the timing of drug delivery to optimize their efficiency and decrease their side effects (*19*).

Since metabolism is an integral part of the circadian machinery (*20*, *21*), energy metabolism should oscillate accordingly. Although debated, several studies report regional and circadian changes in energy metabolism in healthy humans, as measured by positron emission tomography, functional magnetic resonance imaging, magnetic resonance spectroscopy, and glucose sensing in the cerebrospinal fluid (*22*–*27*). Patients with epilepsy display altered metabolic activity in specific brain regions, important information for diagnosis purposes (*28*). We hypothesized time-dependent changes in energy metabolism in control mice and their alteration in experimental epilepsy. We used the databases we provide in control and experimental

[1]Epileptogenesis Laboratory, Nencki Institute of Experimental Biology of Polish Academy of Sciences, 02-093 Warsaw, Poland. [2]Bioinformatics Laboratory, Nencki Institute of Experimental Biology of Polish Academy of Sciences, 02-093 Warsaw, Poland. [3]Department of Computer Science and Institute for Genomics and Bioinformatics, University of California, Irvine, Irvine, CA 92697-3435, USA. [4]Aix Marseille Univ, INSERM, INS, Inst Neurosci Syst, Marseille, France. [5]Department of Pharmacology, Toxicology and Pharmacy, University of Veterinary Medicine Hannover, Hannover, Germany. [6]Department of Neuropathology, University of Bonn Medical Center, Bonn, Germany. [7]Aix-Marseille Univ, CNRS, CRMBM, Marseille, France. [8]APHM, Hôpital Universitaire Timone, CEMEREM, Marseille, France. [9]Department of Biological Chemistry, University of California-Irvine, Irvine, CA 92697, USA.
*These authors contributed equally to this work.
†Present address: Fork Systems, ul. Broniewskiego 10, 05-850 Duchnice, Poland.
‡Corresponding author. Email: christophe.bernard@univ-amu.fr

epilepsy mice to predict which metabolic pathways may be affected and at what time during the night and day cycle. We verified the predictions experimentally, showing that oxidative phosphorylation and glycolysis, which are the two major energy-producing pathways in the brain, are differentially affected in a time-dependent manner in experimental TLE.

Here, we demonstrate that a large set of genes and proteins oscillates in a circadian manner in the ventral hippocampus of control mice. In the pilocarpine experimental model of epilepsy, more genes and proteins are oscillating, with only one-fourth common to control and epilepsy conditions. Among these differences, we predicted and verified time-dependent alterations in energy metabolism between control and experimental mice. We also found a different circadian regulation of the targets of antiepileptic drugs.

RESULTS

Circadian regulation of genes and proteins in the ventral hippocampus of control mice

We first investigated the expression of genes and proteins collecting hippocampi every 4 hours to obtain six time points. Since the distribution of transcripts is heterogeneous along the dorsoventral axis of the hippocampus (*29*), we focused on its ventral part, which is most epileptogenic in human TLE and experimental models (*16*). Using Affymetrix microarrays and the Jonckheere-Terpstra-Kendall (JTK) algorithm (*30*), we identified 1256 transcripts oscillating in the ventral hippocampus of control mice (Fig. 1A and table S1). Hence, 10% of hippocampal genes are regulated in a circadian manner, as compared to 19% in the SCN (*7*) and 6% in the forebrain (*6*). Data from postmortem human hippocampus suggests that less genes ($n = 659$) are oscillating (*31*). Comparison with the latter study is difficult because investigating circadian rhythms requires a strict control of circadian conditions (e.g., no light exposure during the night), which could not be achieved in the human study. Our results are also consistent with the diurnal regulation of genes in nonhuman primates (*32*). Transcriptome analysis was confirmed with quantitative polymerase chain reaction (qPCR) on selected genes, including some core clock genes (fig. S1). We thus verified our first hypothesis: A large number of transcripts undergo circadian regulations in the ventral hippocampus in control mice.

Using one-way analysis of variance (ANOVA) and a false discovery rate (FDR) of <0.05 followed by cluster analysis and functional analysis with DAVID (The Database for Annotation, Visualization, and Integrated Discovery) (https://david.ncifcrf.gov/), we found 486 transcripts differentially expressed, which could be identified on the basis of biological functions (Fig. 1, A to C). We isolated nine clusters. Whereas oscillating patterns were consistent within each cluster, they were distinct between clusters, with transcripts peaking at different times during the night and day cycle (Fig. 1B).

We then compared the oscillating transcripts found in the hippocampus to those already described in subcortical structures (Fig. 2). As expected, we found a clear overlap of the core clock genes involved in the transcriptional and translational feedback loops in the SCN across all investigated brain regions, including the hippocampus (highlighted in green in Fig. 2). Oscillating core clock genes in the hippocampus included *Per1-3*, *Cry1*, *Arnt1*, *Nr1d1-2*, and *Dbp* (Fig. 3, A and B, and Fig. 2). However, a large set of genes were specifically oscillating in the ventral hippocampus as compared to the other regions (Fig. 2), demonstrating that circadian rhythmicity of genes is brain region dependent.

The analysis of the heatmaps (fig. S2) revealed that gene oscillations were distributed with either very low or very high oscillation amplitude in the control hippocampus (Fig. 4A). Most of the genes with high amplitude oscillations were phase advanced in comparison to the rest of the oscillatory transcripts (Fig. 4A).

Having established the circadian rhythmicity of gene transcripts, we asked whether similar properties could be found at the protein level. Proteomic data enabled the analysis of 1500 peptides. We found 170 peptides oscillating in control hippocampi (table S2), i.e., the same percentage (11%) as for gene transcripts. Nine proteins were oscillating in both proteomic and transcriptome datasets. The rather small overlap between the transcriptome and proteome datasets is due to the following reasons. Numerous genes were below detection levels and did not have correspondence in the proteome dataset [e.g., histone deacetylase 1 (HDAC1) and HDAC2 are not represented in the transcriptome dataset]. Conversely, proteins were identified with at least two peptides (with at least one peptide unique to the protein). We applied relatively stringent criteria to control for false positives: We used the "posterior error probability" for each spectrum match (peptide identification) to filter for 1% FDR on a spectrum-match level. We were, therefore, quite conservative to avoid false positives and thus lost some sensitivity. RNA microarrays are targeting predefined transcripts, while the mode of measurement for proteome analyses is untargeted and suffers from stochastic sampling. In addition, proteome favors the most abundant proteins, not the most biologically interesting ones. Despite this, we found the same percentage of oscillating proteins as for gene transcripts.

Together, these results demonstrate that 10% of the gene/protein map in the ventral hippocampus of control mice undergoes a continuous remapping during the night/day cycle. We then performed the same analysis in age-matched TLE mice to determine whether this circadian regulation was modified in pathological conditions.

Altered circadian regulation of genes and proteins in the hippocampus in experimental TLE

In experimental TLE (pilocarpine model), the number of oscillating transcripts was increased by 30% as compared to control (1650 versus 1256; Fig. 1A and table S3). Only 29% of the oscillating transcripts were common to both control and TLE conditions, demonstrating a large modification of the set of genes displaying circadian oscillations in experimental epilepsy. Cluster analysis of differentially expressed genes in control or TLE animals clearly separated the different groups by time and function (Fig. 1B). We thus verified our second hypothesis: The circardian oscillations of gene transcripts are modified in experimental epilepsy as compared to control. The modification involves a large shift toward a different molecular oscillating landscape.

The core clock genes all gained in oscillation amplitudes in TLE as compared to control (Fig. 3, A and B). Many important circadian-related genes gained oscillatory activity in TLE, from which we highlighted Bhlhe40 and Bhlhe41 (Figs. 3B and 4B). Bhlhe40 and Bhlhe41 have been shown to be components of a separate negative feedback loop with Clock/Bmal1. Given that Bhlhe40 and Bhlhe41 have binding sites identified upstream of Per1 and Per2 from MotifMap [FDR < 0.25, Bayesian branch length score (BBLS) of >1.0], increased oscillations of Bhlhe40 and Bhlhe41 may play a key role in the larger recruitment of oscillating transcripts in TLE (*33*, *34*). It will be important to understand the causes and consequences of increased oscillatory activity of core clock genes in TLE.

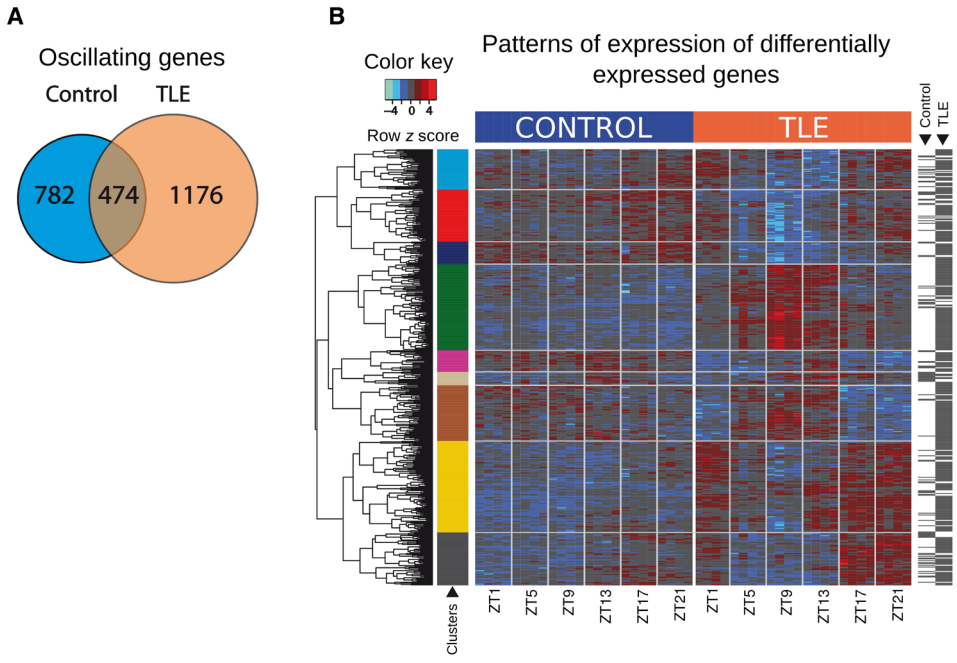

C

Functions of differentially expressed genes

	Term	%	Genes
Cluster 1	Phosphate metabolic process	16 %	MAST2, EIF2AK1, FLT1, ROCK2, ERBB3, WEE1, RNGTT
	Protein phosphorylation	14 %	MAST2, EIF2AK1, FLT1, ROCK2, ERBB3, WEE1
	Protein folding	7 %	GM6568, HSP90B1, AHSA1
Cluster 2	Regulation of transcription	19 %	IRAK2, ZFP329, RBL2, HEXIM1, GABPA, ZFP760, HMG2 HDAC8, ZFP759, ZFP825
	Chromosome organization	10 %	RBL2, HMG20A, HSPA1B, ACIN1, HDAC8
	Response to organic substance	8 %	PHIP, GLUL, DGCR8, STXBP4
Cluster 3	Cell cycle	17 %	CDC7, UHRF2, PRDM5, PLK1S1
Cluster 4	Transmembrane transport	7 %	SLC7A8, KCNA4, MFSD10, SLC25A16, SLC7A5, CACNA1
	Regulation of cell proliferation	7 %	CEBPA, CAV2, FGFRL1, DBH, SOX9, F2R
Cluster 5	Proteolysis	23 %	EML2, QPCT, RAB40C, PSMA7, DNPEP
	Circadian rhythm	9 %	DBP, PER3
Cluster 6	Rhythmic process	15 %	PER2, LFNG
Cluster 7	Translation	8 %	EIF6, MRPS15, LARS, DENR, VARS
	Cellular homeostasis	7 %	GSR, TXNDC11, TFRC, SLC30A1
	Behavior	7 %	NPAS3, UBR3, CCL17, CYR61
Cluster 8	Oxidation reduction	7 %	XDH, DHRS3, FMO2, MAOB, AASS, ASPH, PRODH
	Nucleosome assembly	4 %	HIST1H1E, H2AFV, HIST2H3C2, HIST2H4
Cluster 9	Chromosome organization	11 %	2210018M11RIK, MSL1, HIST1H2BG, HSPA1A, BANP HIST1H3D

Potential regulators of differentially expressed genes

	TRANSCRIPTION FACTOR
Cluster 1	NFY
Cluster 4	Spz1, SMAD, Pax4, LRF, Pax8, ZF5
Cluster 7	ZF5
Cluster 9	ZF5

Fig. 1. Circadian regulation of genes and proteins in the hippocampus and their reprogramming in epilepsy. (**A**) Transcripts oscillating in circadian rhythm. In control mice [$n = 4$ per zeitgeber time (ZT)], 1256 transcripts are oscillating. In TLE ($n = 4$ per ZT), more transcripts are oscillating (1650). Only 474 are common to both conditions, showing a remodeling of the landscape of oscillating genes in TLE. (**B**) Heatmap of 486 mRNAs showing circadian differential expression. Sixty-seven mRNAs were differentially expressed in at least one time point only in control animals, 384 mRNAs were differentially expressed only in TLE, and 35 mRNAs were differentially expressed in both groups. Each column per time window represents an individual animal, and each row represents an individual mRNA. Colors on the heatmap represent *z* score: higher, red; lower, blue. The hour of tissue collection is indicated below (ZT). The dendrogram obtained from hierarchical clustering is shown on the left side of the heatmap. Genes are ordered by clustering complete linkage method together with Pearson correlation distance measure. Colors in the bar on the left side of the heatmap represent clusters obtained by cutting dendrogram at selected level heights to obtain nine groups. Black lines in the bar on the right side of the heatmap mark genes showing differences in expression between control or TLE animals based on one-way ANOVA (analysis of variance) [cut-off false discovery rate (FDR) < 0.05]. (**C**) Left: Biological functions for each gene cluster [defined on the heatmap from (A)] according to Gene Ontology vocabulary using DAVID. Only terms, which are represented by more than 5% of genes in a given cluster, are presented in the table. (Right bottom) Transcription factors with binding sites overrepresented in different gene clusters defined on the heatmap from (B).

The database we provide may help addressing these issues to propose working hypotheses. As an example, we noticed that Runx1, a DNA binding regulator, gained statistical significance in TLE (Figs. 3B and 4B). Several studies report that Runx1 regulates core circadian transcription factors (*35*, *36*). Among these, Per1 and Per3 contain statistically significant transcription factor binding sites in the promoter region for Runx1 (*33*). In addition, rhythmic expression of Runx1 in TLE peaks ~4 hours before Per1 and Per2. Since the mean delay between the time when a circadian transcript reaches its peak of expression and the time for the subsequent protein to reach its peak of expression is ~4 hours (*37*), Runx1 may be involved in the amplification of oscillation in TLE. In addition, Runx1 has protein-protein interaction with two key histone deacetylases, Hdac1 and Hdac2. In keeping with this, proteomics revealed oscillatory activity for Hdac1 and Hdac2 in TLE (table S4). Together, these results suggest that the gain in oscillatory activity of key circadian-related genes

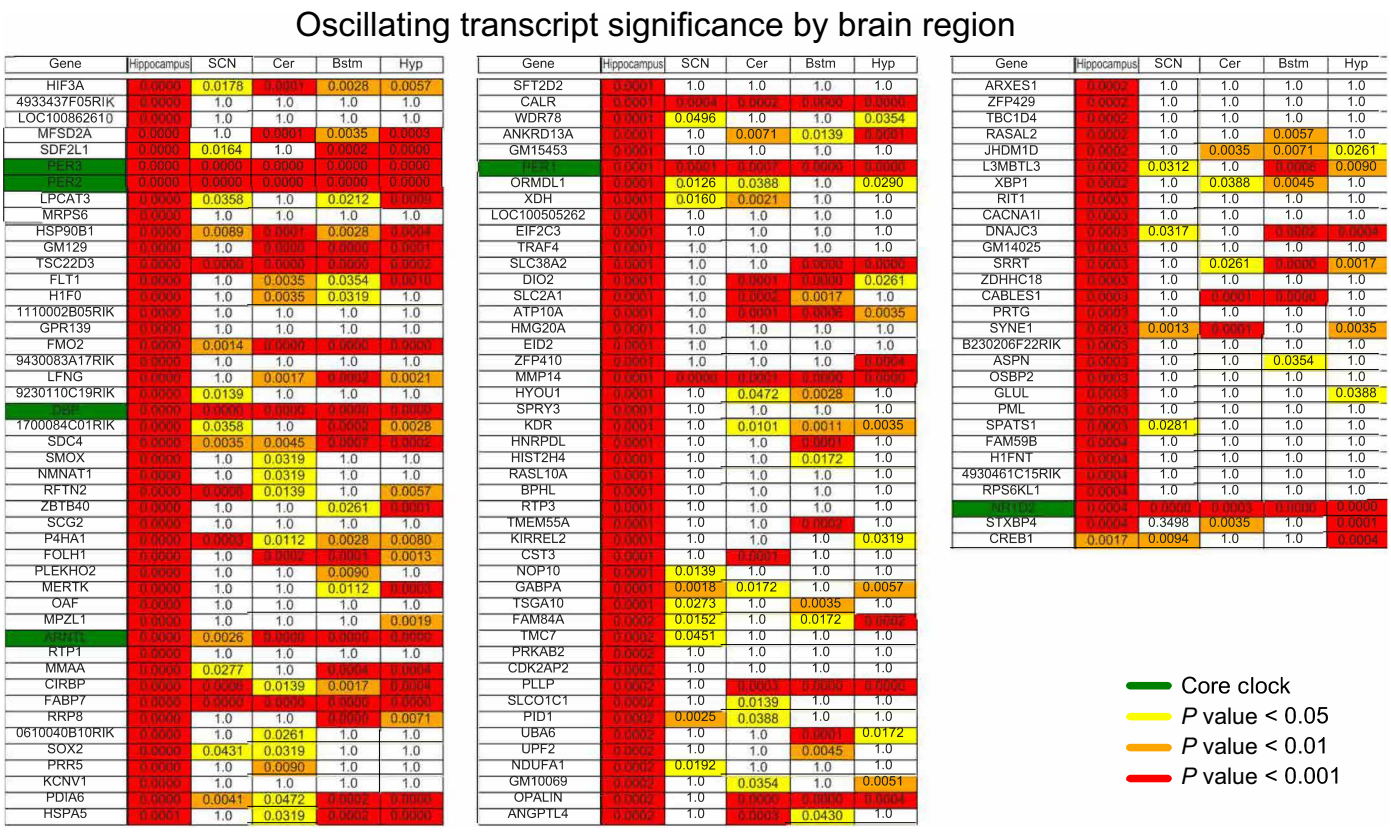

Fig. 2. Comparison of oscillatory transcripts across brain regions. List of genes showing a circadian regulation in control mice, in the hippocampus (hippocampus), SCN, cerebellum (Cer), brainstem (Bstm), and hypothalamus (Hyp). If most core clock genes display circadian regulation in most structures, then numerous genes oscillate specifically in the hippocampus.

in TLE may be driven by regulatory genes starting to oscillate in TLE, such as Runx1. This hypothesis remains to be tested, and the mechanisms underlying the recruitment of Runx1 in TLE warrant further investigation.

The gain in oscillation amplitude was not limited to clock genes in experimental TLE: 705 of the 782 oscillating transcripts showed a greater than 10% increase in amplitude over the average amplitude found in the control condition. For those oscillating transcripts with an increased amplitude, we find proportionally more phase-advanced (defined as a greater than 10% forward shift in phase over the control condition) oscillating transcripts in the TLE-alone condition (Fig. 4B and fig. S2). The dynamics of gene oscillations is thus strongly modified in experimental TLE as compared to control.

We then determined whether similar conclusions are applied at the protein level. As for transcripts, the number of oscillating peptides was increased by 40% in TLE as compared to control (237 versus 170 peptides; Fig. 3C and table S4), with only 5% common to both experimental groups.

We conclude that there is a large change in the daily dynamics of genes and proteins in experimental TLE, as compared to control. Not only the set of oscillating genes is modified but also the amplitude of the oscillation and the phase are changed.

Time-of-the-day–dependent modification of oxidative metabolism and aerobic glycolysis in experimental TLE

The databases we obtained in control and experimental TLE can be used to identify biological processes displaying circadian rhythmicity in the control hippocampus and/or an alteration in experimental TLE. The enriched terms reported from DAVID bioinformatics for oscillating genes found in control condition alone, epileptic condition alone, and oscillating in both conditions for three different *P* values are listed in tables S5 to S13. The gene set enrichment analysis (GSEA) reported many biological pathways showing circadian regulation in control and TLE and specific alterations in TLE, as revealed by KEGG (Kyoto Encyclopedia of Genes and Genomes) (www.genome.jp/kegg/) pathways gene sets, Gene Ontology biological process, Gene Ontology metabolic function, and Reactome (a free, open-source, curated, and peer-reviewed pathway database; https://reactome.org/) (fig. S3 to S14 and table S14 to S25).

This information can be used to identify biological processes that may show circadian alterations in experimental TLE. Since glucose metabolism is altered in patients with TLE and experimental epilepsy (*38*–*42*), we quantified gene set differential expression including gene-gene correlations (*43*) to identify which metabolic pathways may be specifically modified in a circadian manner. Gene sets were selected from Molecular Signatures Database v7.0 [MSigDB; (*44*, *45*)] using the following keywords: "LACTATE.*," "GLYCOLYSIS.*," "GLUCOSE.*," "PENTOSE.*," "CITRIC.*," "GLYCOGEN.*," "PYRUVATE.*," "CIRCADIAN.*," "OXIDATIVE_PHOSPHORYLATION.*," "NEURON_CELLULAR_HOMEO.*," "NEURON_DEATH.*".

We compared the selected gene set activity at each time point for control and TLE animals (Fig. 5A and table S26). Changes in gene sets activity were in the range from 0.87 to 1.30. Values presented on the heatmap are *P* value–based significance score calculated as

A

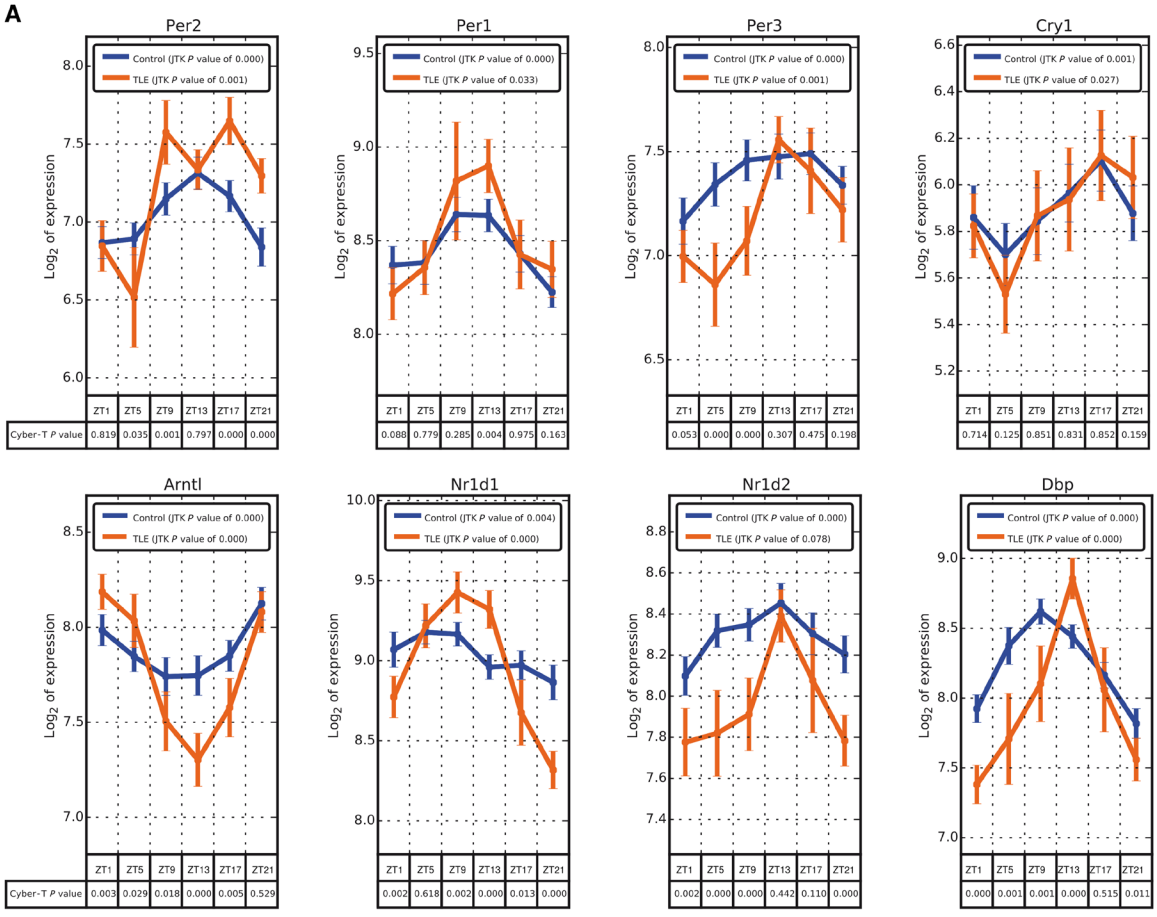

B

Gene	Control amp	Epileptic amp
Bhlhe40	0.2375081574	0.4140875868
Bhlhe41	0.3839730036	0.8064160334
Arntl	0.3834664913	0.8833480509
Hdac8	0.1094111846	0.4769890427
Runx1	0.1811503567	0.7019302037
Per2	0.4750034544	1.130855182
Cry1	0.4035340666	0.5957495958

Fig. 3. Phase change and general increase in oscillation amplitude in TLE, as compared to controls. Oscillation patterns (**A**) and amplitudes (**B**) of core clock genes.

follows: $-\log_{10}(P \text{ value}) \times \text{sign}(\log(\text{fold change}))$. No gene sets displayed constant differences in their activity at all time points, suggesting that circadian regulation in TLE is not paralleled with that of control. Most of the gene sets involved in energy metabolism are slightly less active in TLE, at least at one time point, and their activity is never higher than that in control mice even at zeitgeber time 9 (ZT9) when seizures have the highest probability to occur (Fig. 6A). The activity of gene sets related to glucose uptake and transport, as well as to glycolysis regulation, is slightly down-regulated in TLE at ZT1 only. At all other time points, the activity is similar to control (highlighted in green in Fig. 5A). We, thus, predicted lower glucose utilization at the beginning of the light phase (ZT1 to ZT4) in TLE, followed by a normalization to control levels later on. The heatmap led to a second prediction: Oxidative phosphorylation should be

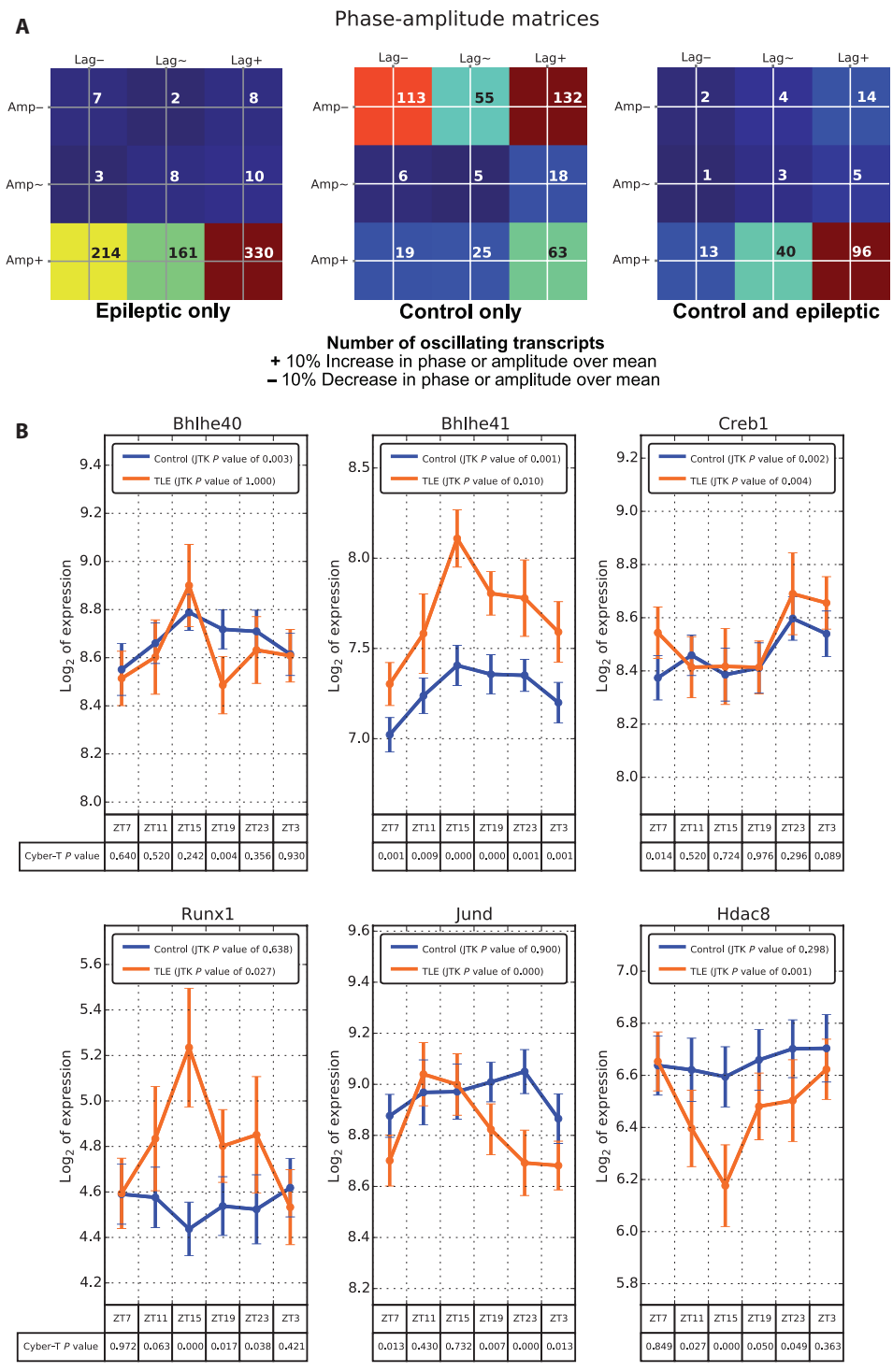

Fig. 4. Different oscillatory patterns of gene transcripts in control mice and their alterations in TLE. (**A**) Phase-amplitude matrices. Most of the transcripts show high amplitude oscillations in TLE, while they are distributed in controls between low and high amplitude. Most of high-amplitude oscillatory transcripts are phase advanced as compared to the rest of the oscillatory transcripts, a property more pronounced in TLE. The number of oscillating transcripts is labeled in each box. Boxes are defined as phase delayed "Lag−," phase advanced "Lag+," or no phase change in the columns. Rows indicate the amplitude. Advanced or delayed amplitude or phase is taken as a minimum of 10% change over the total mean for amplitude and phase, respectively. The number of oscillating transcripts is color coded. Blue indicates the lowest values, and dark red indicates the highest values per condition (control alone, TLE alone, and both). (**B**) Oscillatory patterns of genes that may contribute to the reprogramming of the circadian hippocampal remapping in TLE. *Creb1* oscillates in both conditions. Key controllers of circadian rhythms, *Bhlhe40* and *Bhlhe41*, show increased oscillation amplitudes in TLE, which may contribute to the large recruitment of oscillating genes in TLE. *Runx1*, a DNA binding regulator, and *Hdac8*, a chromatin remodeler, gain statistically significant oscillation in TLE. *JunD* (which interacts with both the AP-1 transcription factor complex and *Creb1*) shows a 180° phase shift in TLE as compared to control.

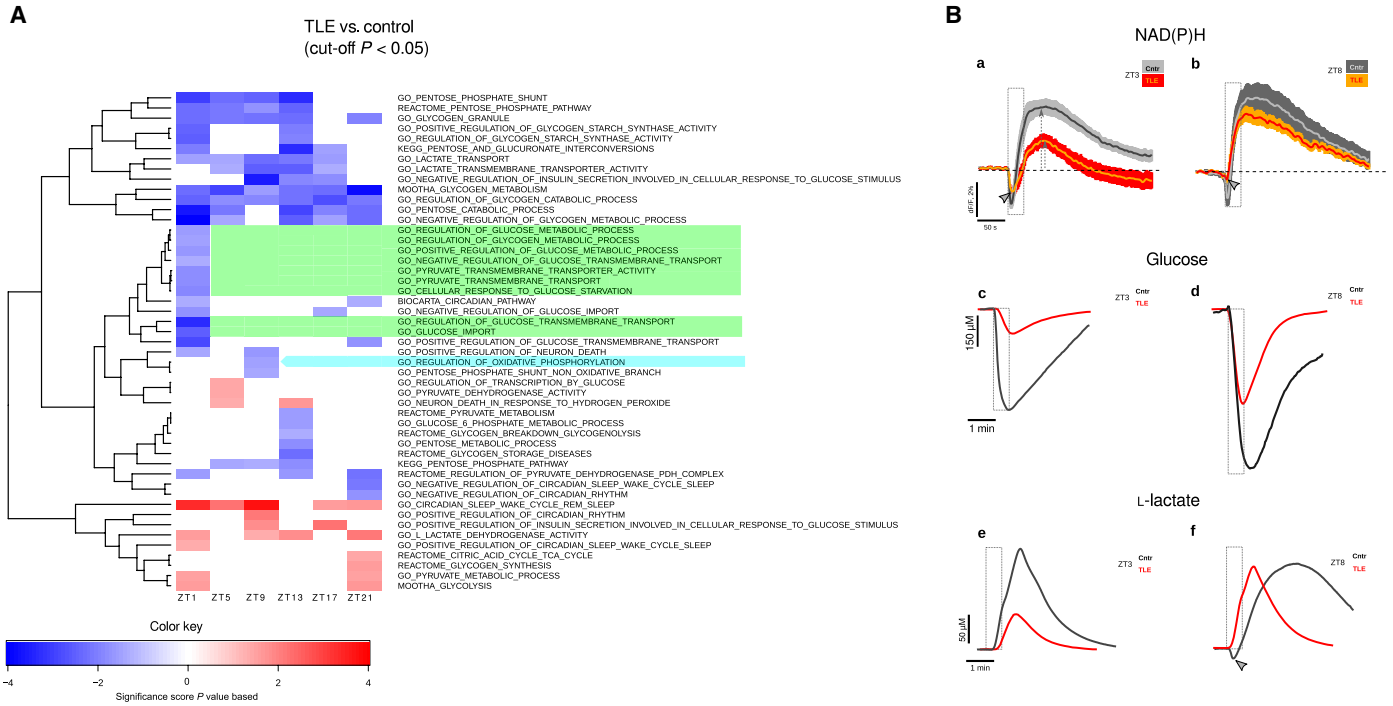

Fig. 5. Alteration of circadian regulation of energy metabolism in TLE. (**A**) Differences between control and TLE animals in selected gene set activity (cut-off *P* value of <0.05). Light green and blue emphasize gene sets involved in glucose aerobic and oxidative metabolism, respectively. (**B**) Metabolic activity induced by electrical stimulation (dashed rectangle) using NAD(P)H (reduced form of nicotinamide adenine dinucleotide phosphate) imaging (a and b), glucose (c and d), and lactate (e and f) sensing. (a) Averaged NAD(P)H fluorescence in TLE (yellow trace) and control (dark gray trace) slices at ZT3. The mean amplitude of the NAD(P)H transient overshoot was significantly smaller in TLE than in control (dashed arrows), suggesting reduced activity of cytosolic glycolysis in TLE. (b) There was no difference in NAD(P)H overshoot in slices prepared at ZT8 in TLE (red trace) and control (gray trace) mice. However, dip amplitudes (gray arrow heads) were significantly smaller in TLE, indicating a reduced activity of oxidative phosphorylation. Glucose consumption (c) and lactate release (e) were lower in TLE (red traces) at ZT3. At ZT8, both parameters were increased in TLE, indicating enhanced aerobic glycolysis activity (d and f, red traces). In control, glucose consumption (d, gray trace) increased with time while lactate release profile (f versus e, gray traces) had lower amplitude as compared to ZT3 and displayed a short-lasting lactate decrease at the beginning of the stimulation (f, gray arrow head).

similar in control and TLE during the ZT1 to 5 time interval but should decrease in TLE at ZT9 (Fig. 5A, light blue arrow).

To test both predictions, we evaluated energy metabolism activity ex vivo in ventral hippocampal slices using two distinct methods, NAD(P)H (reduced form of nicotinamide adenine dinucleotide phosphate) imaging and glucose/lactate sensing during synaptic stimulation. Measurements were performed at ZT3 and at ZT8 on the basis of the predictions (Fig. 5A). Schaffer collateral stimulation produced characteristic transient changes in NAD(P)H fluorescence intensity in the stratum radiatum of the CA1 region: The initial "dip" was followed by the "overshoot" component, reflecting enhanced oxidation and reduction of the pyridine nucleotide, respectively (Fig. 5B, a and b). The overshoot amplitude is related to the intensity of cytosolic glycolysis in both astrocytes and neurons, while the initial dip is associated with mitochondrial oxidative metabolism (*46*). In slices prepared at ZT3 (Fig. 5B, a), the NAD(P)H transient overshoot was significantly smaller in TLE than in control mice (mean amplitude, 1.3 ± 0.17% $n = 9$ versus 3.5 ± 0.5% $n = 10$; $P < 0.01$), suggesting reduced activity of cytosolic glycolysis in TLE as compared to control. However, in slices prepared later, there was no difference in the overshoots [TLE, 4.1 ± 0.4% ($n = 6$); control, 4.6 ± 0.9% ($n = 6$); $P = 0.3$], indicating that glycolytic activity in TLE reached control levels (Fig. 5B, b). This result validates the first prediction. The initial dip of NAD(P)H transient was similar in control slices at both time points (ZT3: −1.9 ± 0.2% versus ZT8: −1.7 ± 0.4; $P = 0.7$, $n = 6$) but was decreased in TLE at ZT8 as compared to ZT3 (−0.6 ± 0.1% versus −1.3 ± 0.2%; $n = 6$, $P < 0.01$; Fig. 5B, b, gray arrowheads), indicating a reduction in the intensity of oxidative phosphorylation, verifying the second prediction.

In the next set of experiments, we used the same experimental conditions and stimulation protocol but measured extracellular glucose or lactate using enzymatic sensors inserted in the stratum radiatum of CA1. Schaffer collateral stimulation triggered a decrease in extracellular glucose, indicating its consumption by cells (Fig. 5B, c and d), leading to an increase of L-lactate in the extracellular space (Fig. 5B, e and f). This indicates that glucose was metabolized to pyruvate that was then partially reduced to L-lactate and finally released. The remaining pyruvate entered the mitochondria to fuel oxidative energy metabolism. At ZT3, glucose consumption was lower in TLE than in control (maximal concentration change, 0.13 ± 0.03 mM versus 0.52 ± 0.14 mM; $P < 0.01$, $n = 9$; Fig. 5B, c), paralleling a smaller amount of released L-lactate (maximal concentration change, 0.04 ± 0.01 mM versus 0.19 ± 0.05 mM; $P < 0.01$, $n = 7$; Fig. 5B, e). Thus, aerobic glycolysis is lower in TLE than in control at ZT3. At ZT8, glucose consumption was increased in both groups (Fig. 5B, d), remaining larger in control as compared to TLE (1.00 ± 0.4 mM versus 0.41 ± 0.08 mM; $P < 0.05$, $n = 5$). Lactate release was increased at ZT8 as compared to ZT3 in TLE [0.12 ± 0.01 mM ($n = 6$) versus 0.04 ± 0.01 mM

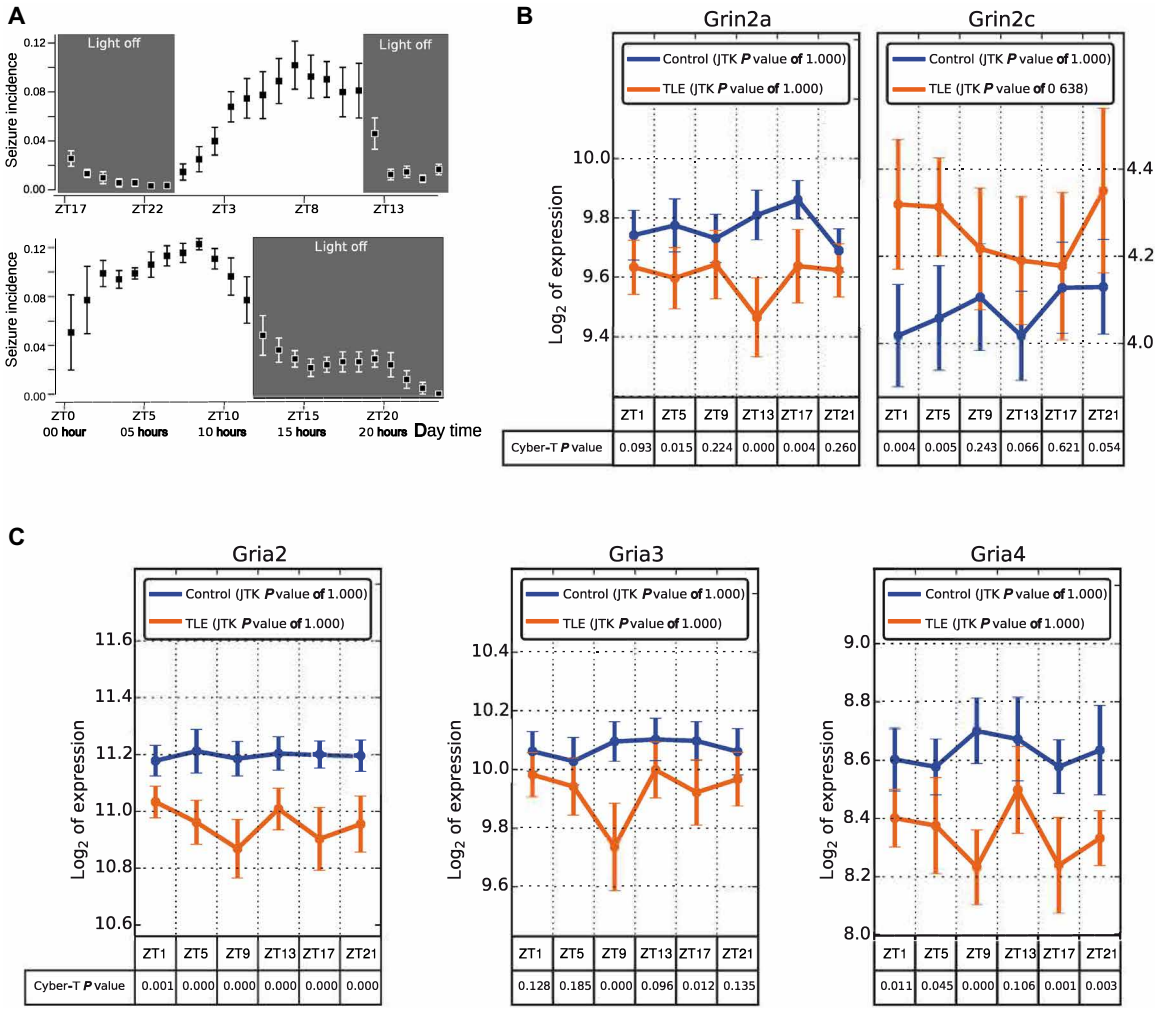

Fig. 6. Circadian regulation of seizures and drug targets in TLE. (**A**) Top: Circadian regulation of seizure incidence during the night and day cycle. The highest seizure probability is found around ZT8. Bottom: Two days after shifting the light/dark cycle by 8 hours in the animal facility, the temporal pattern of seizure incidence shifted accordingly. (**B** and **C**) Alterations of the temporal expression of genes encoding for NMDA (*N*-methyl-D-aspartate) and AMPA receptors subunits, respectively.

($n = 7$); $P < 0.01$), while in control, it tended to decrease at ZT8 as compared to ZT3 [0.11 ± 0.01 mM ($n = 6$) versus 0.19 ± 0.05 mM ($n = 7$); $P = 0.06$).

Together, these results show major time-dependent differences in energy metabolism between TLE and control animals. In TLE, glucose consumption increased together with lactate production, demonstrating enhanced aerobic glycolysis. In controls, lactate release remained unchanged although glucose consumption increased. This means that the intensity of aerobic glycolysis, producing lactate, remained constant, while oxidative metabolism was enhanced via the consumption of additional glucose. Last, we noted that lactate was decreasing at the beginning of synaptic stimulation in controls at ZT8 (Fig. 5B, f, gray arrowhead), indicating either decreased lactate production, because more pyruvate entered into the mitochondria, or lactate uptake and its oxidation to pyruvate. Both scenarios support enhanced oxidative metabolism in controls at ZT8. We conclude that one of the functional consequences of the altered circadian regulation in TLE is a differential, time-dependent recruitment of metabolic pathways. In control conditions, only oxidative metabolism intensity is changing (increasing) between ZT3 and ZT8, while aerobic glycolysis remains constant. In experimental TLE, both oxidative metabolism and aerobic glycolysis are regulated in a time-dependent manner in opposite directions: The oxidative pathway is decreasing and the aerobic glycolysis is increasing between ZT3 and ZT8.

Circadian rhythmicity of seizures and seizure threshold

The circadian rhythmicity can also be appreciated at the system level. Seizures are regulated in a circadian manner in human and experimental mesial TLE (*18*), a result we confirmed in our mouse model (Fig. 6A). Shifting the night and day cycle by 8 hours shifted seizure incidence accordingly (Fig. 6A), demonstrating the circadian rhythmicity of seizures in this model. One explanation could be that the daily remapping of the molecular landscape brings neuronal networks close to seizure threshold at specific time points (*47*). In line with this scenario, we found different seizure susceptibility at different time points between control and TLE animals (fig. S15). This further exemplifies the fact that control and TLE animals operate under different functional regimes.

Consequences for antiepileptic drug targets and chronotherapy

Another possible use of the resource we provide is for drug target design and chronotherapy. Many common drugs (e.g., for gastritis, chronic pain, asthma, and rheumatoid arthritis) target products of genes characterized by circadian rhythmicity (*4*). We obtained information on drugs and genes from the DrugBank database version 5.0.6 (a unique bioinformatics and cheminformatics resource that combines detailed drug data with comprehensive drug target information; www.drugbank.ca/) (*48*), which contains information about 8283 drugs including 62 drugs that exert antiepileptic and anticonvulsant effects. In the database, we found mammalian genes encoding 2230 drug targets, 35 drug carriers, 238 drug enzymes, and 130 drug transporters. For the 62 antiepileptic/anticonvulsant drugs, we found genes encoding 102 drug targets, 1 drug carrier, 32 drug enzymes, and 18 drug transporters.

Among the genes that oscillate in control and TLE animals (JTK_CYCLE, an efficient nonparametric algorithm for detecting rhythmic components in genome-scale datasets, adjusted $P < 0.05$), we found 24 and 71 drug targets, 2 and 2 drug carriers, 2 and 7 drug enzymes, and 2 and 9 drug transporters, respectively (Table 1). There was little overlap between control and experimental TLE datasets, further highlighting the necessity to take into account the specific reorganization of gene oscillations in experimental TLE. We obtained similar conclusions when looking at genes which expression changes (one-way ANOVA; FDR < 0.05) in at least one time point in control and TLE animals. We found 20 and 62 drug targets, 2 and 0 drug carriers, 2 and 11 drug enzymes, and 2 and 7 drug transporters, respectively (Table 1). Table 2 provides examples of oscillating and differentially expressed gene products controlled by antiepileptic and anticonvulsant drugs. Last, new classes of antiepileptic drugs targeting AMPA and *N*-methyl-D-aspartate (NMDA) receptors are being developed (*49*). Many of the corresponding genes of AMPA and NMDA subunits present in the database showed different expression patterns at specific time points in TLE as compared to control (Fig. 6, B and C).

Together, these results suggest that the effects of antiepileptic and anticonvulsant drugs may be time dependent. It is important to stress that drug efficacy testing must be performed in experimental models of chronic epilepsy, as the time-dependent regulation of the drug targets are different in TLE and control conditions. The resource we provide can be used to assess this factor. Whether results obtained in this rodent model can be translated to humans remains to be determined.

DISCUSSION

We conclude that the ventral hippocampus undergoes a complex daily remapping at the gene and protein level, which is different between control and experimental TLE mice. The number of oscillating genes and proteins is likely to be an underestimate in both conditions, as hippocampal samples were collected every 4 hours. Another limitation of our approach is to lump all cell types from the different hippocampal subfields. Future studies should focus on cell type–specific analysis (*50*). In addition, we could not account for the cell loss that is present in TLE models, which may shift the ratios

Table 1. List of genes that oscillate (JTK_CYCLE–adjusted $P < 0.05$) or are differentially expressed during circadian cycle (one-way ANOVA, FDR < 0.05) in control animals and/or experimental TLE. Genes are separated in drug targets, carriers, enzymes, and transporters. There is little overlap between the control and TLE conditions (common ones are underlined). The ABCC1 is not only transporter for phenobarbital but also a drug target for sulfinpyrazone and biricodar dicitrate (in italics). Genes in boldface are shown in Table 2.

Type of action	Oscillating genes	Oscillating genes	Expression change	Expression change
	Control	TLE	Control	TLE
Target	ADAM10, BPHL, **CACNA1I**, CALR, CRBN, FLT1, FOLH1, GLUL, HSP90B1, HSPA5, IGF1R, KDR, MERTK, MMAA, MMP14, NDUFA1, NDUFA6, NMNAT1, NPEPPS, P4HA1, PRKAB2, RAB8B, SMOX, XDH	***ABCC1***, ACAN, ADRBK1, ADSSL1, AFG3L2, AKT2, ALAS1, ALDH6A1, ALKBH3, ANO1, APRT, BCL2, CD52, CTSK, CYB5R3, CYSLTR2, DDAH2, DHPS, DNPEP, EDNRB, F2R, FASN, FPGS, GARS, GLS, GLUL, GPT2, GRIK5, GRM7, GSR, HCN2, HDAC6, HDAC8, HIF1AN, HRH3, IMPG2, LARS, MAPT, MERTK, MLLT4, MMAA, MMP14, MTRR, NDUFA10, NFKBIA, PDE7A, PFN1, PIK3CA, PRKAB1, PSMA4, PSMA7, PSMB7, PTPRS, QPCT, RAB8B, RNGTT, RPL19, RPS6KA4, RYR2, SGPL1, SHMT1, SLC15A2, SLC16A3, SLC6A9, SLC7A8, STMN4, SULT2B1, TSTA3, TUBD1, VARS, WEE1	ADAM10, BRAF, CALR, CXCR4, FLT1, FOLH1, GLUL, HSP90B1, HSPA5, MERTK, MMAA, NDUFA1, NDUFA6, NFKBIA, P4HA1, PRKAB2, SLC16A1, SMOX, TOP1, XDH	AASS, ***ABCC1***, ADSSL1, AGT, AKT2, ALDH6A1, ALDH7A1, AMT, APRT, ASPH, CACNA1B, CALR, CD44, CYB5R3, CYSLTR2, DBH, DDAH2, DDX6, DHPS, DHRS3, DNPEP, F2R, **GABRA3**, GLUL, GPT2, GSR, GSTM5, HDAC6, HDAC8, HIF1AN, HSP90B1, HSPA5, HSPB1, IMPG2, KCNA4, LARS, **MAOB**, MERTK, MLLT4, MMAA, NCOA5, NDUFA10, NFKBIA, P4HA1, PAICS, PDE7A, PDK4, PRKAB1, PRODH, PSMA7, PTPRS, QPCT, RB1, RNGTT, ROCK2, SERPINF2, SHMT1, SLC7A8, SULT2B1, TUBD1, VARS, WEE1
Carrier	FABP7, SLC2A1	FABP5, SLC2A1	FABP7, SLC2A1	
Enzyme	GLUG, XDH	APRT, FPGS, GLS, GLUL, GSR, HIF1AN, VARS	GLUL, XDH	APRT, CHKA, DBH, GLUL, GSR, HIF1AN, MAOB, PRODH, SRM, TGM1, VARS
Transporter	SLC2A1, **SLCO1C1**	**ABCC1**, ABCC5, SLC15A2, SLC16A3, SLC2A1, SLC2A9, SLC7A5, SLC7A8, TFRC	**SLC16A1**, SLC2A1	**ABCC1**, ABCC5, SLC14A1, SLC2A9, SLC7A5, SLC7A8, TFRC

Table 2. Circadian regulation of drug targets and transporters. Genes that are drug target (T) or transporters (Tr) and that oscillate (JTK_CYCLE, adjusted *P* value < 0.05; OSC) or that are differentially expressed (DE) (one-way ANOVA, adjusted *P* value < 0.05; DE) in control (CTR) or TLE animals. Information on drugs can be found in the Supplementary Materials.

Gene symbol	Function	OSC	DE	Animals	Anticonvulsant drug names
ABCC1	Tr	+	+	TLE	Phenobarbital
CACNA1B	T	–	+	TLE	Gabapentin and levetiracetam
CACNA1I	T	+	–	CTR	Paramethadione, zonisamide, and flunarizine
GABRA3	T	–	+	TLE	Meprobamate, metharbital, thiopental, primidone, diazepam, methylphenobarbital, estazolam, fludiazepam, and nitrazepam
MAOB	T	–	+	TLE	Zonisamide
SLC16A1	Tr	–	+	CTR	Valproic acid
SLCO1C1	Tr	+	–	CTR	Phenytoin

between cell types. In addition, we could not distinguish between cell compartments (in neurons, the expression of proteins is different in the dendrites, soma, and axon). Although mixing samples from different forebrain regions, the synaptic transcriptome, proteome, and phosphorylome display strong dynamical modifications driven by the sleep-wake cycle for many more genes and proteins than in the present study (*5*, *6*). By mixing cell types and cell compartments, we may have further underestimated the number of oscillating genes. Since the molecular landscape oscillates in a circadian manner in the hippocampus, it becomes important to take into account the time of the day to study biological processes in this region, as shown for energy metabolism. The circadian oscillation of the molecular landscape of the hippocampus may provide an entry point to study the already known circadian-dependent hippocampal processes and functions.

The origin of these molecular oscillations remains to be determined. They could be a downstream consequence of those occurring in the SCN and the daily activation of various hormonal and neuromodulator pathways (*51*). Alternatively, the clock could be intrinsic, as some hippocampal genes continue to oscillate ex vivo (*52*). Since multiple other damped (secondary) circadian oscillators exist in other brain regions, each with specific phase properties (*53*), it is likely that a remapping also exists in other areas, each with a specific set of regulated genes and proteins. In particular, it will be interesting to analyze the dorsal hippocampus, which gene architecture is different from the ventral hippocampus (*29*).

In experimental epilepsy, we report important modifications in the cycling of genes and proteins, with the possible involvement of epigenetic mechanisms (*54*, *55*). It is not yet possible to determine whether this is a cause or consequence of seizures, altered sleep/wake cycles, or only a homeostatic mechanism. In addition, since mice were kept in colonies to reduce social isolation–induced stress (*56*), it was not possible to assess when each of them had a spontaneous seizure. Although we are not aware of any study reporting a change in gene/protein expression following a spontaneous seizure in a chronic model of TLE, we cannot rule out this possibility.

On the basis of the database, we predicted and verified experimentally a change in the time-dependent regulation in metabolic activity in experimental TLE as compared to control. Whether this alteration in energy production is a compensatory mechanism or whether it is involved in seizure genesis (or comorbidities such as cognitive deficits and depression) remains to be determined. If our results can be translated to patients, then it means that the time of the day becomes a critical factor to consider when performing brain imaging to assess metabolic activity in patients. The fact that circadian changes in metabolism are different between healthy individuals and patients with depression (*57*) supports the proposal that the dynamics of brain metabolism are different in pathological conditions as compared to control, an essential parameter to consider for mechanistic studies.

An important conclusion of the present work is that the ventral hippocampus uses a different functional regime in experimental TLE as compared to control. This makes comparing genes and proteins between control and TLE tissues very difficult, as down- or up-regulation could only sign different oscillating properties in both conditions (e.g., a phase shift). Said differently, a given protein may be down-regulated at time t in TLE as compared to control but up-regulated at time $t + \Delta t$, which renders the functional interpretation of the observation more complicated. On the basis of this novel information, it will be now important to indicate the circadian time a given animal was used in any experimental condition and to take into consideration possibly altered gene/protein rhythmicity. The fact that targets of antiseizure drugs and seizure threshold oscillate differently in control and TLE conditions support the idea that regions in health and disease may operate under different functioning modes.

In conclusion, the possibility that the molecular landscape of neuronal networks may oscillate in a circadian manner in all brain regions offers interesting new avenues of research. It is also possible that such altered circadian rhythmicity occurs in most (if not all) neurological disorders (*58*). This possibility is important to consider for chronotherapeutics (*59*).

MATERIALS AND METHODS

Animals

All experiments were performed on FVB adult male mice following INSERM procedures. All animals had the same age (less than 1 week difference), and tissue collection was performed when animals were 14 weeks old. Twenty-four control and 24 TLE mice were used for transcriptomics and proteomics. They were kept in a special in-house animal facility with a strict control of light and temperature conditions (beginning of the light phase at 7:30 and beginning of the night phase at 1930). A red light, which does not disrupt circadian rhythmicity, was present during the night phase to allow researchers to manipulate the animals. During the night phase, no external light could enter the room when opening the door. Mice were housed in groups of four to five to enable social interaction. Cages had enriched environment. Throughout the experimental procedure, the same researcher took care of the animals at the same time of the day to limit external stressful factors. Animals were anesthetized with isoflurane in the animal facility, and four of them were sacrificed every 4 hours (six time points).

The brain was quickly extracted, and the hippocampus was removed in modified ice-cold artificial cerebrospinal fluid (ACSF). Right (for transcriptome analysis) and left (for proteomics) extracted hippocampi were separated into two halves, i.e., ventral and dorsal parts, and quickly frozen. Only the ventral parts were used here. The average time between decapitation and sample freezing was 90 s per mice to limit any degradation of gene products and proteins. All tissue collection was performed during a single 24-hour period. The collection of the hippocampal tissue from the four mice per time window was performed in less than 10 min.

Model of epilepsy

Adult FVB mice were injected with methylscopolamine [1 mg/kg, intraperitoneally (ip)] 30 min before the pilocarpine injections. Pilocarpine was repeatedly injected (100 mg/kg, ip), every 20 min, until status epilepticus (SE) was observed. After 90 min of SE, we injected diazepam (10 mg/kg, ip) to stop SE. All mice then received 0.5 ml of NaCl (0.9%) subcutaneously and again in the evening. During the following days, if required, then mice were fed using a syringe.

24/7 EEG monitoring

Ten mice were implanted with a telemetry probe [ETA-F10, Data Science International (DSI), St Paul, MN] for electroencephalography (EEG) analysis only (the brain was not harvested for transcriptome or connectome analysis). The stereotaxic surgery was performed under ketamine (100 mg/kg)/xylazine (10 mg/kg) anesthesia. Lidocaine was used locally. Temperature, heart rate, and breathing rate were continuously monitored during the surgical procedure using MouseOx Plus monitor (Starr Life Sciences Corp., Oakmont, PA, USA). A recording skull screw was secured above the hippocampal CA1 region (−1.8 mm posterior, +1.8 mm lateral), and a reference skull screw was secured above the cerebellum. The leads of the DSI telemetry probe (DSI, St Paul, MN) were wrapped around the recording and reference screws, and the screws were all encased in dental cement. The probe body containing the battery was subcutaneously placed in the back of the mice. Animals were allowed 7 days of post-surgical recovery before any further experimental procedures were conducted. EEG recordings were continuously performed until the end of the experimental protocol. Seizures were automatically detected with a DSI software (adjusting for frequency and amplitude) using low detection values. This led to numerous false positives (mostly movement artifacts), which were manually removed after double checking by a trained technician and clinical epileptologist. Complete EEG recordings were fully visually inspected. No false negatives were detected (i.e., the semi-automated procedure insured the detection of all seizures). All pilocarpine-treated mice developed spontaneous seizures.

Animal care and handling

We kept six mice (control or epileptic) per cage, with enriched environment. We found that keeping epileptic mice together (as opposed to one mouse per cage) markedly changed their behavior. They recovered faster from SE. They could be easily handled, denoting a lack of stress. When epileptic mice are housed in individual cages, they are extremely nervous, and it is very difficult to handle them. Here, we removed a confounding stress factor linked to the lack of social interaction, as reported in rats (*56*).

Seizure threshold tests with pentylenetetrazole

Seizure threshold was determined in individual male FVB mice by the timed intravenous pentylenetetrazole (PTZ) test, as described previously (*60*), in a total of 57 naive and 55 epileptic mice. Epilepsy was induced by pilocarpine (*61*), and seizure thresholds were determined 7 to 9 weeks after SE, when all mice had developed epilepsy. Groups of 8 to 20 mice were used per threshold determination. PTZ infusion was stopped at the first seizure, and seizure threshold was calculated in milligrams of PTZ per kilogram of body weight on the basis of the infusion time needed to induce this seizure end point (*60*). PTZ thresholds were determined every 4 hours during the light and dark phase. The maximum number of threshold determinations was limited to three per animal with 7 days in between (repeated seizure threshold tests do not alter the threshold if an interval of at least 48 hours lies within the determinations) (*60*, *62*, *63*). In addition, we performed two PTZ seizure threshold determinations at the same time point (ZT4:30) to compare PTZ thresholds at the beginning and at the end of the experiment, demonstrating the reproducibility of the method.

Data were analyzed by using the Prism 5 software (GraphPad, La Jolla, CA, USA). Thresholds of the control and SE animals were separately analyzed using one-way ANOVA and Bonferroni post hoc tests and combined by using a two-way ANOVA with Student's *t* tests as post hoc analysis. All tests that were used were two sided; a $P < 0.05$ was considered significant.

RNA isolation and microarray hybridization

The isolation of total RNA was performed using the miRNeasy Mini kit (QIAGEN, no. 217004) according to the manufacturer's instructions. The sample quality was determined using a NanoDrop 2000 spectrophotometer (Thermo Fisher Scientific), and Agilent 2100 Bioanalyzer. GeneChip Mouse Gene 2.1 ST arrays (Affymetrix, Santa Clara, CA; no. 902120) were used for mRNA profiling. Total mRNA (100 ng) was used for complementary DNA synthesis using the Ambion WT Expression Kit (Life Technologies, no. 4411974). Hybridization, washing, and scanning were conducted according to the Affymetrix guidelines for the GeneAtlas instrument.

Quantitative PCR

Reverse transcription for individual qPCRs was carried out using 250 ng of total RNA and the High-Capacity Reverse Transcription

Kit (no. 4368814, Life Technologies) according to the manufacturer's instruction. qPCRs were run on the ABI 7900HT Fast Real-Time PCR instrument (Applied Biosystems). Gene expression analysis was conducted using a relative standard curve method with glyceraldehyde-3-phosphate dehydrogenase to normalize the expression levels of target genes. All reactions were performed in triplicates.

Bioinformatic analysis

Analysis of microarrays was performed using R/Bioconductor (R Core Team, 2014; www.bioconductor.org). All microarrays were normalized with the robust multi-array average algorithm using oligo package (version 1.28.3). Background value of intensity of probes was defined as the median value of the intensity of antigenomic probes. The intensity of genomic probes below the background intensity was corrected to this background value. Probes with intensity greater than the background value in less than four samples were removed from analysis. Only probes that corresponded to a single gene were selected for further analysis.

JTK_CYCLE and BIO_CYCLE were used to identify oscillating genes at three *P* value thresholds (*30*). Gene lists for transcripts oscillating at each *P* value in the control condition alone, the TLE condition alone, or both conditions were identified for further analysis. Cyber-T was used to identify differentially expressed transcripts between control and TLE conditions in each time point (*64*). Cyber-T *P* values found for each time point for core clock genes are reported (Fig. 3A). Proteomic data for both control and TLE conditions was also analyzed by JTK_CYCLE to identify rhythmic proteins. All transcriptome data is available for search on CircadiOmics along with JTK_CYCLE and BIO_CYCLE results (*65*).

Genes, which expression level differed between time points according to one-way ANOVA analysis performed separately for control and epileptic animals, are presented on the heatmap (Fig. 1B). Differences were considered as significant for adjusted $P < 0.05$ (FDR–Benjamini and Hochberg correction). Genes were ordered by clustering complete linkage method together with Pearson correlation distance measure. Nine gene clusters highlighted on the heatmap were obtained by cutting dendrogram the selected level of the dendrogram. Functional analysis for biological function Gene Ontology terms was performed using the MF FAT Chart option with default settings in DAVID [http://david.abcc.ncifcrf.gov; (*12*, *13*)]. The GSEA (http://software.broadinstitute.org/gsea/index.jsp) was performed on the basis of gene sets obtained from MSigDB v5.0 (http://software.broadinstitute.org/gsea/msigdb/index.jsp). For GSEA, a ranking based score $-\log_{10}(P \text{ value}) \times \text{sign}(\text{fold change})$ was used. *P* values and fold changes were obtained from comparisons with *t* test between two consecutive time points in control and TLE animals separately (figs. S3 to S8) or between control and TLE animals at each time point (figs. S9 to S14). The GSEA was performed with weighted enrichment statistic, meandiv normalization mode, max probe collapsing mode, and with min/max size restriction (10/1000). Gene sets were considered as down- or up-regulated whether nominal $P < 0.05$ and FDR < 0.25. Transcription factor binding sites overrepresented in promoters within clusters were detected with g:Profiler [http://biit.cs.ut.ee/gprofiler/; (*66*, *67*)] with custom background defined as genes detected in the experiment to reveal the functional and regulatory groups presented in the data.

Further transcription factor binding site enrichment analysis was performed using MotifMap (*33*, *68*) and chromatin immunoprecipitation sequencing (ChIP-seq) datasets provided by University of California Santa Cruz (UCSC) Encode project (*69*). Transcription factor binding sites identified by MotifMap were found both 10-kb upstream and 2-kb downstream of transcription start sites (TSSs) for all genes in each of the differentially expressed gene lists for all pair-wise comparisons. The motifs identified were found with a BBLS conservation score of greater than or equal to 1.0 and an FDR of less than 0.25. ChIP-seq datasets were used to locate experimentally identified binding site locations within the same interval around the TSS for differentially expressed genes. Only the 90th percentile of ChIP-seq peaks was used from each dataset provided by the UCSC Encode. A Fisher's exact test was performed separately using the full background list of motifs from MotifMap and all target genes from the ChIP-seq datasets to compute the statistical likelihood of overrepresentation in promotor regions.

The qusage package (version 2.20.0; http://bioconductor.org/packages/release/bioc/html/qusage.html) was used to perform the quantitative set analysis for gene expression (*43*). Gene sets were obtained from MSigDB v7.0 (*44*, *45*). Sets were selected using the following patterns: LACTATE.*, GLYCOLYSIS.*, GLUCOSE.*, PENTOSE.*, CITRIC.*, GLYCOGEN.*, PYRUVATE.*, CIRCADIAN.*, OXIDATIVE_PHOSPHORYLATION.*, NEURON_CELLULAR_HOMEO.*, NEURON_DEATH.*. The *P* value–based significance score was calculated as follows: $-\log_{10}(P \text{ value}) \times \text{sign}(\log(\text{fold change}))$. *P* value of less than 0.05 was considered significant.

Proteomics

Protein extraction

All steps of the protein extraction were performed on ice or at 4°C. Isolated hippocampal tissue was homogenized in lysis buffer containing 20 mM triethylammonium bicarbonate (TEAB; Fluka), 5% sodium deoxycholate (SDC; Sigma-Aldrich), and one tablet of protease inhibitor (Roche). Homogenates were boiled for 3 min and subsequently sonicated three times for 10 s, each time paused for 30 s. Samples were centrifuged to pellet tissue debris, and the protein concentration in the supernatant was measured with a bicinchoninic acid protein assay (Pierce) using bovine serum albumin as standard.

Protein digestion

Dithiotreitol (DTT) was added to 200 μg of the global protein fraction up to a final concentration of 20 mM DTT in the solution. Samples were incubated for 20 min at 55°C and then centrifuged for 1 min at 10,000*g* (20°C). The supernatant was transferred to filter devices (10 kDa molecular weight cut off, VWR) and filled up with digestion buffer (DB) containing 20 mM TEAB and 0.5% SDC. Next, the samples were centrifuged for 10 min at 10,000*g* (20°C), the flow-through was discarded, and 100 μl of 40 mM indoacetamide in DB was added to the filter devices followed by a 20-min incubation at room temperature in darkness. Afterward, samples were washed twice with DB, and trypsin solved in DB was added to yield a protein-to-trypsin ratio of 100:1. Samples were incubated overnight at 37°C. Filter devices were centrifuged for 20 min at 10,000*g* (20°C), and the flow-through was collected. Residual peptides were removed by another centrifugation step with DB. The flow-throughs of one sample were combined, and, first, an equal volume of ethyl acetate and subsequently trifluoroacetic acid (final concentration 0.5%) were added. The solution was mixed and centrifuged for 2 min at 14,000*g* (20°C). The upper layer was discarded, and 250 μl of ethyl acetate was added, followed by centrifugation. The upper layer was discarded again, and the aqueous phase was collected for further procession.

Isobaric labeling and peptide fractionation

Peptides were vacuum concentrated and labeled with amine-reactive, six-plex tandem mass tag reagents (Thermo Fisher Scientific, Bremen, Germany) according to the manufacturer's instructions. The labeling reaction was quenched by the addition of 5% hydroxylamine. Labeled peptides were pooled and desalted on Oasis HLB cartridges (Waters GmbH, Eschborn, Germany). Eluates containing 70% acetonitrile and 0.1% formic acid were dried and fractionated to 24 fractions by isoelectric point using an OFFGEL fractionator according to the manufacturer's recommendations (Agilent Technologies, Waldbronn, Germany). Peptide fractions were dried and stored at −20°C.

Liquid chromatography–mass spectrometry analysis

Peptides were dissolved in 8 μl of 0.1% trifluoroacetic acid, and 1.5 μl was injected onto a C18 trap column (20 mm in length, 100 μm in inner diameter) coupled to a C18 analytical column (200 mm in length, 75 μm in inner diameter), made in house with 1.9 μm of ReproSil-Pur 120 C18-AQ particles (Dr. Maisch, Ammerbuch, Germany). Solvent A was 0.1% formic acid. Peptides were separated during a linear gradient from 4 to 40% solvent B (90% acetonitrile and 0.1% formic acid) within 90 min. The nano–high-performance liquid chromatography was coupled online to an LTQ Orbitrap Velos mass spectrometer (Thermo Fisher Scientific). Peptide ions between 330 and 1800 mass/charge ratio (m/z) were scanned in the Orbitrap detector with a resolution of 30,000 (maximum fill time of 400 ms, AGC (automatic gain control) target of 10^6, and lock mass of 371.0318 Da). The 20 most intense precursor ions (threshold intensity of 5000) were subjected to higher energy collision–induced dissociation, and fragments were also analyzed in the Orbitrap. Fragmented peptide ions were excluded from repeat analysis for 15 s. Raw data processing and analyses of database searches were performed with Proteome Discoverer software 1.4.1.12 (Thermo Fisher Scientific). Peptide identification was done with an in-house Mascot server version 2.4.1 (Matrix Science Ltd., London, UK). MS2 data (including a-series ions) were searched against mouse sequences from Swiss-Prot (release 2014_01). Precursor ion m/z tolerance was 10 parts per million; fragment ion tolerance was 20 mmu (milli mass unit). Tryptic peptides were searched with up to two missed cleavages. Low scoring spectrum matches were searched again with semitryptic specificity with up to one missed cleavage. Oxidation (Met), acetylation (protein N terminus), and TMTsixplex (on Lys and N terminus) were set as dynamic modifications; carbamidomethylation (Cys) was set as static modification. Mascot results from searches against Swiss-Prot were sent to the percolator algorithm (*70*) version 2.04, as implemented in Proteome Discoverer. Only proteins with two peptides (maximum FDR of 1%) were considered as identified.

In vitro experiments

Tissue slice preparation

Mice were anaesthetized with isoflurane and decapitated at ZT4 or ZT8. The brain was rapidly removed from the skull and placed in the ice-cold ACSF as above. The ACSF solution consisted of the following: NaCl (126 mM), KCl (3.50 mM), NaH_2PO_4 (1.25 mM), $NaHCO_3$ (25 mM), $CaCl_2$ (2.00 mM), $MgCl_2$ (1.30 mM), and dextrose (5 mM) (pH 7.4). ACSF was aerated with 95% O_2/5% CO_2 gas mixture. Slices of ventral hippocampus (350 μm) were cut, as described (*62*), using a tissue slicer (Leica VT 1200 S, Leica Microsystem, Germany). The ice-cold (<6°C) cutting solution consisted of the following: K-gluconate (140 mM), Hepes (10 mM), Na-gluconate (15 mM), EGTA (0.2 mM), and NaCl (4 mM), pH adjusted to 7.2 with KOH. Slices were then immediately transferred to a multisection, dual-side perfusion holding chamber with constantly circulating ACSF and allowed to recover for 2 hours at room temperature (22° to 24°C). Slices were then transferred to a recording chamber continuously superfused with ACSF (flow rate of 7 ml/min, warmed at 30° to 31°C) with access to both slice sides.

Synaptic stimulation and field potential recordings

Schaffer collaterals were stimulated using a DS2A isolated stimulator (Digitimer Ltd., UK) with a bipolar metal electrode. Stimulus current was adjusted using single pulses (100 to 250 μA, 200 μs, 0.15 Hz) to induce a local field potential (LFP) of about 60% of the maximal amplitude. LFPs were recorded using glass microelectrodes filled with ASCF, placed in stratum pyramidale, and connected to an EXT-02F/2 amplifier (NPI Electronic GmbH, Germany). Synaptic stimulation, consisting of a stimulus train (200-μs pulses) at 10 Hz lasting 30 s, was used to trigger metabolic response.

NAD(P)H fluorescence imaging and extracellular glucose/lactate measurement

NADPH and reduced form of nicotinamide adenine dinucleotide (NAD^+) (NADH) have similar optical properties; therefore, it is expected that NADPH may contribute to the total autofluorescence signal. Because the cellular $NADP^+$/ NADPH pool is about one order of magnitude lower than the NAD/NADH pool, in the present study, we assume that short-term variations of experimentally detected fluorescent change responses account for variations in NADH [see discussion in (*71*)]. Here, for the fluorescent signal, we use the term NAD(P)H. Changes in NAD(P)H fluorescence in hippocampal slices were monitored using a 290- to 370-nm excitation filter and a 420-nm long-pass filter for the emission (Omega Optical, Brattleboro, VT). The light source was the pE-2 illuminator (CoolLed, UK) equipped with 365-nm light-emitting diode. Slices were epi-illuminated and imaged through a Nikon upright microscope (FN1, Eclipse) with 4×/0.10 Nikon Plan objective. Images were acquired using a 16-bit Pixelfly CCD (charge-coupled device) camera (PCO AG, Germany). Because of a low level of fluorescence emission, NAD(P)H images were acquired every 600 to 800 ms as 4 × 4 binned images (effective spatial resolution of 348 × 260 pixels). The exposure time was adjusted to obtain baseline fluorescence intensity between 30 and 40% of the CCD dynamic range. Fluorescence intensity changes in the stratum radiatum near the site of the LFP recording were averaged from three regions of interest >500-μm distant from the stimulation electrode tip using the ImageJ software [National Institutes of Health (NIH), USA]. Data were expressed as the percentage changes in fluorescence over a baseline [$(\Delta F/F) \bullet 100$]. Signal analysis was performed using the Igor Pro software (WaveMetrics Inc., OR, USA).

Tissue glucose and lactate concentrations were measured with enzymatic microelectrodes (tip diameter of 25 μm; Sarissa Biomedical, Coventry, UK), polarized at 0.5 V, and driven with free radical analyzer TBR4100 (WPI, USA). Calibration was performed before and after each slice recording, and the recorded data were corrected for eventual changes in electrode sensitivity. To avoid an interaction between enzymatic electrodes, glucose and lactate measurements were performed in separate sets of experiments.

Statistical analysis and signal processing

NAD(P)H dip and overshoot amplitudes and maximal changes in extracellular glucose/lactate concentrations were expressed as means ± SEM. Normality was rejected by Shapiro-Wilk normality test, and

we used nonparametric Wilcoxon rank sum test. The level of significance was set at $P < 0.05$.

SUPPLEMENTARY MATERIALS

Supplementary material for this article is available at http://advances.sciencemag.org/cgi/content/full/6/41/eaat5979/DC1

View/request a protocol for this paper from *Bio-protocol*.

REFERENCES AND NOTES

1. J. Bass, M. A. Lazar, Circadian time signatures of fitness and disease. *Science* **354**, 994–999 (2016).
2. S. Masri, P. Sassone-Corsi, The circadian clock: A framework linking metabolism, epigenetics and neuronal function. *Nat. Rev. Neurosci.* **14**, 69–75 (2013).
3. K. Eckel-Mahan, P. Sassone-Corsi, Metabolism and the circadian clock converge. *Physiol. Rev.* **93**, 107–135 (2013).
4. R. Zhang, N. F. Lahens, H. I. Ballance, M. E. Hughes, J. B. Hogenesch, A circadian gene expression atlas in mammals: Implications for biology and medicine. *Proc. Natl. Acad. Sci. U.S.A.* **111**, 16219–16224 (2014).
5. F. Brüning, S. B. Noya, T. Bange, S. Koutsouli, J. D. Rudolph, S. K. Tyagarajan, J. Cox, M. Mann, S. A. Brown, M. S. Robles, Sleep-wake cycles drive daily dynamics of synaptic phosphorylation. *Science* **366**, eaav3617 (2019).
6. S. B. Noya, D. Colameo, F. Brüning, A. Spinnler, D. Mircsof, L. Opitz, M. Mann, S. K. Tyagarajan, M. S. Robles, S. A. Brown, The forebrain synaptic transcriptome is organized by clocks but its proteome is driven by sleep. *Science* **366**, eaav2642 (2019).
7. V. L. Harbour, Y. Weigl, B. Robinson, S. Amir, Comprehensive mapping of regional expression of the clock protein PERIOD2 in rat forebrain across the 24-h day. *PLOS ONE* **8**, e76391 (2013).
8. L. E. Chun, E. R. Woodruff, S. Morton, L. R. Hinds, R. L. Spencer, Variations in phase and amplitude of rhythmic clock gene expression across prefrontal cortex, hippocampus, amygdala, and hypothalamic paraventricular and suprachiasmatic nuclei of male and female rats. *J. Biol. Rhythms* **30**, 417–436 (2015).
9. C. A. Barnes, B. L. McNaughton, G. V. Goddard, R. M. Douglas, R. Adamec, Circadian rhythm of synaptic excitability in rat and monkey central nervous system. *Science* **197**, 91–92 (1977).
10. K. M. Harris, T. J. Teyler, Age differences in a circadian influence on hippocampal LTP. *Brain Res.* **261**, 69–73 (1983).
11. D. Chaudhury, L. M. Wang, C. S. Colwell, Circadian regulation of hippocampal long-term potentiation. *J. Biol. Rhythms* **20**, 225–236 (2005).
12. R. G. Munn, D. K. Bilkey, The firing rate of hippocampal CA1 place cells is modulated with a circadian period. *Hippocampus* **22**, 1325–1337 (2012).
13. R. G. Munn, S. M. Tyree, N. McNaughton, D. K. Bilkey, The frequency of hippocampal theta rhythm is modulated on a circadian period and is entrained by food availability. *Front. Behav. Neurosci.* **9**, 61 (2015).
14. P. Li, X. Fu, N. A. Smith, J. Ziobro, J. Curiel, M. J. Tenga, B. Martin, S. Freedman, C. A. Cea-del Rio, L. Oboti, T. N. Tsuchida, C. Oluigbo, A. Yaun, S. N. Magge, B. O'Neill, A. Kao, T. G. Zelleke, D. T. Depositario-Cabacar, S. Ghimbovschi, S. Knoblach, C. Y. Ho, J. G. Corbin, H. P. Goodkin, S. Vicini, M. M. Huntsman, W. D. Gaillard, G. Valdez, J. S. Liu, Loss of CLOCK results in dysfunction of brain circuits underlying focal epilepsy. *Neuron* **96**, 387–401.e6 (2017).
15. H. C. Matos, B. D. V. Koike, W. D. S. Pereira, T. G. de Andrade, O. W. Castro, M. Duzzioni, M. Kodali, J. P. Leite, A. K. Shetty, D. L. G. Gitaí, Rhythms of core clock genes and spontaneous locomotor activity in post-*Status Epilepticus* model of mesial temporal lobe epilepsy. *Front. Neurol.* **9**, 632 (2018).
16. I. Toyoda, M. R. Bower, F. Leyva, P. S. Buckmaster, Early activation of ventral hippocampus and subiculum during spontaneous seizures in a rat model of temporal lobe epilepsy. *J. Neurosci.* **33**, 11100–11115 (2013).
17. M. Langdon-Down, W. R. Brain, Time of day in relation to convulsions in epilepsy. *Lancet* **213**, 1029–1032 (1929).
18. M. Quigg, M. Straume, M. Menaker, E. H. Bertram III, Temporal distribution of partial seizures: Comparison of an animal model with human partial epilepsy. *Ann. Neurol.* **43**, 748–755 (1998).
19. S. Ramgopal, S. Thome-Souza, T. Loddenkemper, Chronopharmacology of anti-convulsive therapy. *Curr. Neurol. Neurosci. Rep.* **13**, 339 (2013).
20. F. Gachon, U. Loizides-Mangold, V. Petrenko, C. Dibner, Glucose homeostasis: Regulation by peripheral circadian clocks in rodents and humans. *Endocrinology* **158**, 1074–1084 (2017).
21. C. M. Greco, P. Sassone-Corsi, Circadian blueprint of metabolic pathways in the brain. *Nat. Rev. Neurosci.* **20**, 71–82 (2019).
22. M. M. Verbeek, W. G. Leen, M. A. Willemsen, D. Slats, J. A. Claassen, Hourly analysis of cerebrospinal fluid glucose shows large diurnal fluctuations. *J. Cereb. Blood Flow Metab.* **36**, 899–902 (2016).
23. O. Al-Iedani, J. Arm, K. Ribbons, R. Lea, J. Lechner-Scott, S. Ramadan, Diurnal stability and long-term repeatability of neurometabolites using single voxel 1H magnetic resonance spectroscopy. *Eur. J. Radiol.* **108**, 107–113 (2018).
24. J. Arm, O. Al-Iedani, R. Lea, J. Lechner-Scott, S. Ramadan, Diurnal variability of cerebral metabolites in healthy human brain with 2D localized correlation spectroscopy (2D L-COSY). *J. Magn. Reson. Imaging* **50**, 592–601 (2019).
25. B. J. Shannon, R. A. Dosenbach, Y. Su, A. G. Vlassenko, L. J. Larson-Prior, T. S. Nolan, A. Z. Snyder, M. E. Raichle, Morning-evening variation in human brain metabolism and memory circuits. *J. Neurophysiol.* **109**, 1444–1456 (2013).
26. D. J. Buysse, E. A. Nofzinger, A. Germain, C. C. Meltzer, A. Wood, H. Ombao, D. J. Kupfer, R. Y. Moore, Regional brain glucose metabolism during morning and evening wakefulness in humans: Preliminary findings. *Sleep* **27**, 1245–1254 (2004).
27. E. J. Bartlett, J. D. Brodie, A. P. Wolf, D. R. Christman, E. Laska, M. Meissner, Reproducibility of cerebral glucose metabolic measurements in resting human subjects. *J. Cereb. Blood Flow Metab.* **8**, 502–512 (1988).
28. J. S. Duncan, G. P. Winston, M. J. Koepp, S. Ourselin, Brain imaging in the assessment for epilepsy surgery. *Lancet Neurol.* **15**, 420–433 (2016).
29. C. L. Thompson, S. D. Pathak, A. Jeromin, L. L. Ng, C. R. MacPherson, M. T. Mortrud, A. Cusick, Z. L. Riley, S. M. Sunkin, A. Bernard, R. B. Puchalski, F. H. Gage, A. R. Jones, V. B. Bajic, M. J. Hawrylycz, E. S. Lein, Genomic anatomy of the hippocampus. *Neuron* **60**, 1010–1021 (2008).
30. M. E. Hughes, J. B. Hogenesch, K. Kornacker, JTK_CYCLE: An efficient nonparametric algorithm for detecting rhythmic components in genome-scale data sets. *J. Biol. Rhythms* **25**, 372–380 (2010).
31. J. Z. Li, B. G. Bunney, F. Meng, M. H. Hagenauer, D. M. Walsh, M. P. Vawter, S. J. Evans, P. V. Choudary, P. Cartagena, J. D. Barchas, A. F. Schatzberg, E. G. Jones, R. M. Myers, S. J. Watson, H. Akil, W. E. Bunney, Circadian patterns of gene expression in the human brain and disruption in major depressive disorder. *Proc. Natl. Acad. Sci. U.S.A.* **110**, 9950–9955 (2013).
32. L. S. Mure, H. D. le, G. Benegiamo, M. W. Chang, L. Rios, N. Jillani, M. Ngotho, T. Kariuki, O. Dkhissi-Benyahya, H. M. Cooper, S. Panda, Diurnal transcriptome atlas of a primate across major neural and peripheral tissues. *Science* **359**, eaao0318 (2018).
33. K. Daily, V. R. Patel, P. Rigor, X. Xie, P. Baldi, MotifMap: Integrative genome-wide maps of regulatory motif sites for model species. *BMC Bioinformatics* **12**, 495 (2011).
34. B. Bode, R. Taneja, M. J. Rossner, H. Oster, Advanced light-entrained activity onsets and restored free-running suprachiasmatic nucleus circadian rhythms in *Per2/Dec* mutant mice. *Chronobiol. Int.* **28**, 737–750 (2011).
35. F. Lu, Q. Liu, Validation of RUNX1 as a potential target for treating circadian clock-induced obesity through preventing migration of group 3 innate lymphoid cells into intestine. *Med. Hypotheses* **113**, 98–101 (2018).
36. M. E. Reale, I. C. Webb, X. Wang, R. M. Baltazar, L. M. Coolen, M. N. Lehman, The transcription factor Runx2 is under circadian control in the suprachiasmatic nucleus and functions in the control of rhythmic behavior. *PLOS ONE* **8**, e54317 (2013).
37. M. S. Robles, J. Cox, M. Mann, In-vivo quantitative proteomics reveals a key contribution of post-transcriptional mechanisms to the circadian regulation of liver metabolism. *PLOS Genet.* **10**, e1004047 (2014).
38. F. Chassoux, E. Artiges, F. Semah, S. Desarnaud, A. Laurent, E. Landre, P. Gervais, B. Devaux, O. B. Helal, Determinants of brain metabolism changes in mesial temporal lobe epilepsy. *Epilepsia* **57**, 907–919 (2016).
39. T. S. McDonald, C. Carrasco-Pozo, M. P. Hodson, K. Borges, Alterations in cytosolic and mitochondrial [U-^{13}C]glucose metabolism in a chronic epilepsy mouse model. *eNeuro* **4**, ENEURO.0341-16.2017 (2017).
40. S. Vielhaber, J. H. von Oertzen, A. F. Kudin, A. Schoenfeld, C. Menzel, H. J. Biersack, T. Kral, C. E. Elger, W. S. Kunz, Correlation of hippocampal glucose oxidation capacity and interictal FDG-PET in temporal lobe epilepsy. *Epilepsia* **44**, 193–199 (2003).
41. D. E. Kuhl, J. Engel Jr., M. E. Phelps, C. Selin, Epileptic patterns of local cerebral metabolism and perfusion in humans determined by emission computed tomography of ^{18}FDG and $^{13}NH_3$. *Ann. Neurol.* **8**, 348–360 (1980).
42. C. Dubé, S. Boyet, C. Marescaux, A. Nehlig, Relationship between neuronal loss and interictal glucose metabolism during the chronic phase of the lithium-pilocarpine model of epilepsy in the immature and adult rat. *Exp. Neurol.* **167**, 227–241 (2001).
43. G. Yaari, C. R. Bolen, J. Thakar, S. H. Kleinstein, Quantitative set analysis for gene expression: A method to quantify gene set differential expression including gene-gene correlations. *Nucleic Acids Res.* **41**, e170 (2013).
44. A. Liberzon, A. Subramanian, R. Pinchback, H. Thorvaldsdóttir, P. Tamayo, J. P. Mesirov, Molecular signatures database (MSigDB) 3.0. *Bioinformatics* **27**, 1739–1740 (2011).
45. A. Subramanian, P. Tamayo, V. K. Mootha, S. Mukherjee, B. L. Ebert, M. A. Gillette, A. Paulovich, S. L. Pomeroy, T. R. Golub, E. S. Lander, J. P. Mesirov, Gene set enrichment

analysis: A knowledge-based approach for interpreting genome-wide expression profiles. *Proc. Natl. Acad. Sci. U.S.A.* **102**, 15545–15550 (2005).
46. A. I. Ivanov, C. Bernard, D. A. Turner, Metabolic responses differentiate between interictal, ictal and persistent epileptiform activity in intact, immature hippocampus in vitro. *Neurobiol. Dis.* **75**, 1–14 (2015).
47. V. K. Jirsa, W. C. Stacey, P. P. Quilichini, A. I. Ivanov, C. Bernard, On the nature of seizure dynamics. *Brain* **137**, 2210–2230 (2014).
48. V. Law, C. Knox, Y. Djoumbou, T. Jewison, A. C. Guo, Y. Liu, A. Maciejewski, D. Arndt, M. Wilson, V. Neveu, A. Tang, G. Gabriel, C. Ly, S. Adamjee, Z. T. Dame, B. Han, Y. Zhou, D. S. Wishart, DrugBank 4.0: Shedding new light on drug metabolism. *Nucleic Acids Res.* **42**, D1091–D1097 (2014).
49. M. A. Rogawski, W. Löscher, J. M. Rho, Mechanisms of action of antiseizure drugs and the ketogenic diet. *Cold Spring Harb. Perspect. Med.* **6**, a022780 (2016).
50. L. M. Prolo, J. S. Takahashi, E. D. Herzog, Circadian rhythm generation and entrainment in astrocytes. *J. Neurosci.* **25**, 404–408 (2005).
51. B. L. Smarr, K. J. Jennings, J. R. Driscoll, L. J. Kriegsfeld, A time to remember: The role of circadian clocks in learning and memory. *Behav. Neurosci.* **128**, 283–303 (2014).
52. L. M.-C. Wang, J. M. Dragich, T. Kudo, I. H. Odom, D. K. Welsh, T. J. O'Dell, C. S. Colwell, Expression of the circadian clock gene Period2 in the hippocampus: Possible implications for synaptic plasticity and learned behaviour. *ASN Neuro* **1**, e00012 (2009).
53. V. L. Harbour, Y. Weigl, B. Robinson, S. Amir, Phase differences in expression of circadian clock genes in the central nucleus of the amygdala, dentate gyrus, and suprachiasmatic nucleus in the rat. *PLOS ONE* **9**, e103309 (2014).
54. S. McClelland, G. P. Brennan, C. Dubé, S. Rajpara, S. Iyer, C. Richichi, C. Bernard, T. Z. Baram, The transcription factor NRSF contributes to epileptogenesis by selective repression of a subset of target genes. *eLife* **3**, e01267 (2014).
55. K. Kobow, I. Blümcke, Epigenetic mechanisms in epilepsy. *Prog. Brain Res.* **213**, 279–316 (2014).
56. H. Manouze, A. Ghestem, V. Poillerat, M. Bennis, S. Ba-M'hamed, J. J. Benoliel, C. Becker, C. Bernard, Effects of single cage housing on stress, cognitive, and seizure parameters in the rat and mouse pilocarpine models of epilepsy. *eNeuro* **6**, ENEURO.0179-18 (2019).
57. A. Germain, E. A. Nofzinger, C. C. Meltzer, A. Wood, D. J. Kupfer, R. Y. Moore, D. J. Buysse, Diurnal variation in regional brain glucose metabolism in depression. *Biol. Psychiatry* **62**, 438–445 (2007).
58. E. S. Musiek, D. M. Holtzman, Mechanisms linking circadian clocks, sleep, and neurodegeneration. *Science* **354**, 1004–1008 (2016).
59. R. Silver, L. J. Kriegsfeld, Circadian rhythms have broad implications for understanding brain and behavior. *Eur. J. Neurosci.* **39**, 1866–1880 (2014).
60. M. Rattka, C. Brandt, M. Bankstahl, S. Bröer, W. Löscher, Enhanced susceptibility to the GABA antagonist pentylenetetrazole during the latent period following a pilocarpine-induced status epilepticus in rats. *Neuropharmacology* **60**, 505–512 (2011).
61. M. Bankstahl, J. P. Bankstahl, W. Löscher, Pilocarpine-induced epilepsy in mice alters seizure thresholds and the efficacy of antiepileptic drugs in the 6-Hertz psychomotor seizure model. *Epilepsy Res.* **107**, 205–216 (2013).
62. G. M. Pollack, D. D. Shen, A timed intravenous pentylenetetrazol infusion seizure model for quantitating the anticonvulsant effect of valproic acid in the rat. *J. Pharmacol. Methods* **13**, 135–146 (1985).
63. W. Löscher, Preclinical assessment of proconvulsant drug activity and its relevance for predicting adverse events in humans. *Eur. J. Pharmacol.* **610**, 1–11 (2009).
64. M. A. Kayala, P. Baldi, Cyber-T web server: Differential analysis of high-throughput data. *Nucleic Acids Res.* **40**, W553–W559 (2012).
65. V. R. Patel, K. Eckel-Mahan, P. Sassone-Corsi, P. Baldi, CircadiOmics: Integrating circadian genomics, transcriptomics, proteomics and metabolomics. *Nat. Methods* **9**, 772–773 (2012).
66. J. Reimand, T. Arak, J. Vilo, g:Profiler—A web server for functional interpretation of gene lists (2011 update). *Nucleic Acids Res.* **39**, W307–W315 (2011).
67. J. Reimand, M. Kull, H. Peterson, J. Hansen, J. Vilo, g:Profiler—A web-based toolset for functional profiling of gene lists from large-scale experiments. *Nucleic Acids Res.* **35**, W193–W200 (2007).
68. X. Xie, P. Rigor, P. Baldi, MotifMap: A human genome-wide map of candidate regulatory motif sites. *Bioinformatics* **25**, 167–174 (2009).
69. The ENCODE Project Consortium, An integrated encyclopedia of DNA elements in the human genome. *Nature* **489**, 57–74 (2012).
70. L. Käll, J. D. Storey, M. J. MacCoss, W. S. Noble, Assigning significance to peptides identified by tandem mass spectrometry using decoy databases. *J. Proteome Res.* **7**, 29–34 (2008).
71. A. Mayevsky, G. G. Rogatsky, Mitochondrial function in vivo evaluated by NADH fluorescence: From animal models to human studies. *Am. J. Physiol. Cell Physiol.* **292**, C615–C640 (2007).

Acknowledgments
Funding: This work was supported by Inserm, the European Union's Seventh Framework Programme (FP7/2007-2013) under grant agreement no. 602102 (EPITARGET), and A*MIDEX ION project 2IONXXID/REID/ID17HRU208 and ANR-14-CE13-0018-03. W.L. and S.B. are supported by the Niedersachsen-Research Network on Neuroinfectiology (N-RENNT) of the Ministry of Science and Culture of Lower Saxony in Germany. K.J.D. and K.L. are supported by the Polish Ministry of Science and Higher Education grants 888/N-ESF-EuroEPINOMICS/10/2011/0 and W19/7.PR/2014. The work of N.C. and P.B. is, in part, supported by NIH grant GM123558 to P.B. **Author contributions:** A.G., A.M.B., G.E.B., and J.A.M. performed the experiments and analyzed the data. A.B., A.I.I., K.J.D., N.C., S.B., S.S., and W.L. performed the experiments, analyzed the data, and wrote the manuscript. A.B., K.L., P.B., N.C., and P.S.-C. supervised aspects of the project and wrote the manuscript. C.B. conceived and managed the project, performed the experiments, analyzed the data, and wrote the manuscript. **Competing interests:** The authors declare that they have no competing interests**. Data and materials availability:** All data needed to evaluate the conclusions in the paper are present in the paper and/or the Supplementary Materials. All the data are publicly available on the CircadiOmics web portal at http://circadiomics.igb.uci.edu/. Additional data related to this paper may be requested from the authors.

Submitted 15 March 2018
Accepted 27 August 2020
Published 9 October 2020
10.1126/sciadv.aat5979

Citation: K. J. Debski, N. Ceglia, A. Ghestem, A. I. Ivanov, G. E. Brancati, S. Bröer, A. M. Bot, J. A. Müller, S. Schoch, A. Becker, W. Löscher, M. Guye, P. Sassone-Corsi, K. Lukasiuk, P. Baldi, C. Bernard, The circadian dynamics of the hippocampal transcriptome and proteome is altered in experimental temporal lobe epilepsy. *Sci. Adv.* **6**, eaat5979 (2020).